Physics and Chemistry of Minerals manuscript No.
(will be inserted by the editor)

The compressibility and high pressure structure of diopside from first principles simulation

Andrew M. Walker[1], **Richard P. Tyer**[2], **Richard P. Bruin**[1], **Martin T. Dove**[1]

[1] Department of Earth Sciences, University of Cambridge, Downing Street, Cambridge, CB2 3EQ, UK

[2] STFC Daresbury Laboratory, Warrington, Cheshire, WA4 4AD, UK

Received: date / Revised version: date

Abstract The structure of diopside ($CaMgSi_2O_6$) has been calculated at pressures between 0 and 25 GPa using the planewaves and psudopotentials approach to Density Functional Theory. After applying a pressure correction of 4.66 GPa to allow for the under-binding usually associated with the Generalized Gradient Approximation, cell parameters are in good agreement with experiment and fitting to the third order Birch-Murgahan equation of state yields values of 122 GPa and 4.7 for the bulk modulus and its

Correspondence to: Andrew M. Walker, e-mail: amw75@cam.ac.uk,

phone: +44 (0)1223 333432, fax: +44 (0)1223 333450

pressure derivative. In addition to cell parameters, our calculations provide all atomic positional parameters to pressures considerably beyond those currently available from experiment. We have analyzed these data in terms of polyhedral rigidity and regularity and find that the most compressible Ca polyhedron becomes markably less anisotropic above 10 GPa.

Key words diopside, density functional theory, equation of state, pyroxene, compression

1 Introduction

Linking compositional models of the Earth's mantle to observed geophysical data requires knowledge of the properties of candidate minerals at high pressure and temperature. Increasingly this information is supplied by first principles simulation, which can circumvent experimental limitations and derive the structure and properties of minerals under extreme conditions while giving atomic-scale insight into important processes. Recent examples of this approach include the development of an Earth reference model based on mineral physics data (Weidner et al., 2006) and an analysis of the mechanism of the water induced weakening of the mantle (Walker et al., 2007). Given this interest and the fact that diopside has historically been seen as a difficult stuture to model (Dove, 1989), it is perhaps surprising that modern electronic structure methods have not been used to determine the high pressure behavior of diopside ($CaMgSi_2O_6$), the magnesium rich

end member of the calcium bearing clinopyroxenes found in the Earth's crust and upper mantle. However, such methods have been used to probe the electron distribution in diopside, e.g. Gibbs et al. (2005) and Bianchi et al. (2005). Here, we rectify this by reporting results derived from density functional theory which reveal the equation of state and high pressure structure of diopside.

The compressibility and compression mechanism of diopside have been studied experimentally on a number of occasions. Levien and Prewitt (1981) compressed a natural single crystal to 5 GPa in a diamond anvil cell and recovered full structure refinements from X-ray diffraction. McCormick et al. (1989) and Zhang et al. (1997) also performed single crystal X-ray diffraction in diamond anvil apparatus, compressing natural and synthetic samples to 6 and 10 GPa, respectively. More recently Rietveld refinement of data from X-ray powder diffraction experiments have recovered the cell parameters of diopside to 40 GPa (Tribaudino et al., 2000). However, the crystal structure could not be determined at this pressure. Indeed, until very recently, the only published high pressure structure refinements were those of Levien and Prewitt (1981). New experiments reported by Thompson and Downs (2008), provide structural data to 10 GPa. This data, which was collected from a natural single crystal compressed in a diamond anvil cell, is consistent with the results of Levien and Prewitt (1981) and Tribaudino et al. (2000) but differs from the results of Zhang et al. (1997).

Like all pyroxenes the structure of diopside is characterized by parallel chains of corner sharing silicon tetrahedra (Si) and edge sharing octahedra (M1) parallel to the c axis (Figures 1a and 1b). These essential structural elements are embedded in a pseudo-close packed array of oxygen atoms with sheets of oxygen atoms parallel to (100). In diopside the oxygen atoms are arranged with distorted cubic close packing (CCP) with three symmetrically distinct oxygen sites and a third cation site (M2). The M1 site is occupied by magnesium while the M2 site is occupied by eight-coordinated calcium. One oxygen site (O3) is shared between adjacent tetrahedra while a second (O2) lies in the same (100) sheet as the two O3 atoms bonded to its silicon atom. The third, apical, oxygen (O1) bonded to each silicon is in the adjacent (100) plane and links parallel chains of Si and Mg atoms. The two Si–O3 bonds have slightly different bond lengths, and we call the longer bond Si–O3a and the shorter bond Si–O3b. Similally, there are two Mg–O1 bond lengths, Mg–O1b being longer then Mg–O1a. The Ca polyhedra also form kinked edge sharing chains (Figures 1c and 1d). There are two pairs of Ca–O3 bonds in the structure, with Ca–O3a being longer then Ca–O3b.

The CCP oxygen sub-lattice is actually extremely distorted and was the most distorted of the common rock forming minerals studies by Thompson and Downs (2001). In a hypothetical pyroxene with perfect CCP oxygen sub-lattice the space group would be $C2/c$, one would expect the tetrahedera and octehedera to be perfectly regular, and the Si–O–Si angle would be 120° (Thompson and Downs, 2003, 2004). Although diopside does crystalize in

the $C2/c$ space group, the bond lengths are not equivalent. All four Si–O bonds are different lengths with the two inequivalent bonds to bridging oxygen being shorter then the two non-bridging bonds. There are three pairs of inequivalent Mg–O bonds in the M1 octahedera and four inequivalent Ca–O bonds around the M2 site. Previous experimental analysis of the structural evolution with pressure is based on the data of Levien and Prewitt (1981) who show that the M2 site is the most compressible cation site, and the Si site the least compressible. Thompson and Downs (2001) showed that the effect of pressure was to drive the structure towards more perfect close packing while Thompson et al. (2005) was able to fit the compressibility to a simple model driven by the evolution of oxygen ion radius and O3–O3–O3 angle (Figure 1a).

2 Methodology

Our calculations made use of Density Functional Theory (DFT; Hohenberg and Kohn, 1964; Kohn and Sham, 1965), an exact recasting of the time independent Schrödinger equation for electrons in the potential field of nuclei, to evaluate the energy of a periodic model of diopside. Although DFT is an exact theory the exchange correlation functional is not known and must be approximated. We made use of the functional of Perdew et al. (1996), which belongs to the family of functionals within the generalized gradient approximation (see Jung and Oganov, 2005, for a recent review of these methods).

The calculations were performed using the popular planewaves and pseudopotentials approach for DFT-based models of periodic systems, which owes much to the work of Car and Parrinello (1985). The key feature of this approach is to represent the core and valence electrons in different ways so that most of the computational effort is concentrated on the behaviour of the valence electrons. These are represented by a planewave basis expansion that includes all waves whose kinetic energy, $E_k = \hbar^2 k^2 / 2m$ (m is the electron mass, k is the wavevector), is less then a cutoff energy threshold. In our calculations a cutoff of of 600 eV was used. Core electrons were described by ultrasoft psudopotentials fitted to all election GGA results for isolated atoms (Vanderbilt, 1990). Electrons in the 2s and 2p, 2p and 3s, 3s and 3p, and 3s, 3p and 4s levels were treated as valance states for O, Mg, Si and Ca atoms, respectively. All lower levels were treated as core states. The Brillouin zone was sampled with a 2×2×2 Monkhorst-Pack grid (Monkhorst and Pack, 1976) which was fine enough to converge the total energy and forces on the atoms (shown in the supplementary information).

Using this approach the enthalpy, cell volume and structure of diopside were calculated at pressures from 0 to 25 GPa in increments of 1 GPa. For each pressure all internal degrees of freedom were allowed to vary along with the cell parameters during minimization of the energy.

We made use of the CASTEP code (Segall et al., 2002) to perform the calculations. The calculations were run in parallel on the four clusters belonging to the North-West Grid (Thomas et al., 2007) and each made use

of 32 compute cores connected by a high performance ethernet-based SCore interconnects. Typical run times were of the order of 12 (wall clock) hours.

3 Results

The calculated cell parameters at each pressure increment are reported in Table 1 and compared with experiment in Figure 2. Comparison of the 0 GPa result with neutron diffraction data collected at 4 K (Prencipe et al., 2000) shows that the calculated results overestimate the a, b, c and β cell parameters by 1.8, 1.7 and 1.7 % and 0.8°, respectively. This overestimate in cell volume (and a corresponding decrease of the elastic stiffness and vibrational frequencies) compared to experiment is typical of calculations making use of the GGA but the uniform nature of the expansion is gratifying. For comparison, an equivalent calculation at 0 GPa using the local density approximation yielded cell parameters that were too small (underestimated a, b, c and β by 0.9, 1.3 and 1.0 % and 0.03°, respectively).

As expected, fitting the calculated pressure – volume (P–V) data to the third order Birch-Murnaghan equation of state:

$$P = \frac{3K_0}{2}\left[\left(\frac{V_0}{V}\right)^{7/3} - \left(\frac{V_0}{V}\right)^{5/3}\right] \times \left\{1 + \frac{3\left(K_0' - 4\right)}{4}\left[\left(\frac{V_0}{V}\right)^{2/3} - 1\right]\right\}, \quad (1)$$

with the zero pressure volume, V_0, bulk modulus, K_0, and its pressure derivative, K_0', as free parameters gives a solution: $V_0 = 458.0$ Å^3, $K_0 = 99.8$ GPa, and $K_0' = 4.9$, which is softer than experimental values of $V_0 = 439.13$

± 0.06 Å^3, $K_0 = 113 \pm 3$ GPa, $K_0' = 4.8 \pm 0.7$ (Levien and Prewitt, 1981), $V_0 = 439.465 \pm 0.016$ Å^3, $K_0 = 105.1 \pm 0.9$ GPa, $K_0' = 6.8 \pm 0.1$ (Tribaudino et al., 2000) and $V_0 = 438.66 \pm 0.02$ Å^3, $K_0 = 118 \pm 1$ GPa, $K_0' = 3.8 \pm 0.2$ (Thompson and Downs, 2008).

The anisotropy of the compression of the unit cell with pressure is revealed by the unit strain ellipsoid as a function of pressure. This is calculated using the STRAIN software (Ohashi, 1982) and is represented in Figure 3 and Table 1 of the supplementary material. The distortion is measured from the unit cell at the indicated pressure and that at 0 GPa with ε_2 parallel to the crystallographic b axis and ε_1 and ε_3 in the ac–plane. This data is qualitatively similar to the strain calculated from experiment (Thompson and Downs, 2008) but the strain is too high at low pressure. This is due to the underbinding associated with the GGA. The general trend is for strong anisotropy in the ac–plane (ε_1 and ε_3 are very different).

In addition to the cell parameters the calculations also yield atomic positions at each pressure. Although no point symmetry was imposed on the calculations (all 40 atoms were free to move in any direction if this reduced the system's enthalpy) the system retained $C2/c$ symmetry. Atomic positions for the atoms in the asymmetric unit are given in Table 2. This data is also available in Crystallographic Information File (.cif) format as supplementary information.

We extracted information regarding the three distinct coordination polyhedera from the crystal structure; the evaluation of bond lengths and poly-

hedral volume with pressure are shown in Supplementary Tables 2, 3 and 4. We also identify the center and radius, r, of the sphere that minimizes the distance from the vertex atoms to the sphere surface using the approach described by Balić Žunić and Makovicky (1996). The best fitting sphere yields two measures of polyhedral distortion reported in Table 3. The first, Δ, is the deviation of the central atom from the center of the best fit sphere. For a perfect polyhedera this displacement is zero. The second measure, called the sphericity, Σ, is derived from the standard deviation, σ_r, of the distances from the sphere center to the co-ordinating atoms and is given by: $\Sigma = (1 - \sigma_r/r)$. In a regular polyhedera all the atoms lie exactly on the surface of the sphere and this measure is equal to 1 (it is also equal to 1 for any tetrahedera). These two measures of polyhedral regularity do not account for deviations in the shape of the coordination polyhedera. One can imagine moving the atoms on the surface of the best fit sphere without changing r, Δ or Σ. Makovicky and Balić-Žunić (1998) provide a way to quantify this type of deviation by comparing the volume of the polyhedera with the volume of the equivalent regular polyhedera inscribed by a sphere of radius r. As the polyhederal shape moves away from the perfect equivalent its volume will tend to decrease. The shape deformation can thus be quantified by the volume discrepancy, $\upsilon(\%) = (V_i - V_r)/V_i \times 100$. Finally, we also evaluate the compressibility of the three polyhedera by fitting third order Birch-Murnaghan equation of state to the polyhederal volumes.

For the Si tetrahedera we extract equation of state parameters $V_0 = 2.26$ Å^3, $K_0 = 334.4$ GPa and $K_0' = 6.4$ and the bond length evolution is shown in Figure 4. Notable observations are that the anisotropy of the bond lengths is retained over the whole pressure range, with bonds to the bridging oxygen atoms always shorter than non bridging bonds. The Si–O–Si bond angle becomes monotonously more kinked over the whole pressure range while the two measures of polyhederal distortion, Δ and υ initially decreases a little with increasing pressure before distortion increases again. The minimum distortion occurs at 12 GPa.

The Mg site is much softer with the EOS fit giving parameters $V_0 = 12.63$ Å^3, $K_0 = 88.9$ GPa and $K_0' = 4.3$. The intermediate length Mg–O1b bond is least compressible, Figure 5. The displacement of the central atom from the center of the octahedron decreases with pressure, while the shape of the octahedron becomes increasingly distorted. In terms of Σ, the minimum distortion of bond lengths is at 12 GPa, about the pressure when the length of the intermediate length bond is midway between the other two bond lengths.

Calcium occupies the most compressible M2 site and fitting its volume to the EOS yields $V_0 = 27.1$ Å^3, $K_0 = 75.3$ GPa and $K_0' = 4.8$. At ambient pressure the bond length compressabilities are very anisotropic with the longest Ca–O3a bond being by far the most compressible bond in the structure, Figure 6. Indeed, by 20 GPa this bond is shorter then the Ca–O3b bond. At all pressures the central atom is significantly more displaced from

the centroid then in the case of the tetrahedera or octahedera, and increasing pressure decreases this displacement. Increasing pressure also increases sphericity. In order to derive the volume discrepancy of the Ca polyhedera it is first necessary to define an ideal shape. For this we take the Archamedian square antiprism (Makovicky and Balić-Žunić, 1998, Table 2). The maximum volume discrepancy of this site occurs at 14 GPa, with a minimum distortion at 1 GPa. One of the interesting observations is that the Ca polyhedron becomes less anisotropic with increasing pressure, as shown by Figure 6, and by the decrease in volume discrepancy and centroid displacement, and increase in sphericity with pressure. The results presented here do not allow us to distinguish if this regularization drives or is driven by the compression mechanism of diopside. However, Thompson and Downs (2008) point out that a simple model including isotropic scaling and tetrahedral rotation reproduce most of this trend, suggesting that the rapid shortening does not control the compressibility.

4 Discussion and Conclusions

As mentioned above, our simulations result in cell parameters that are too large and a compressibility that is too high when compared to experiment. In order to arrive at a more reasonable estimate of the equation of state we follow Vanderbilt (1998) and Oganov et al. (2001) and apply an empirical pressure correction to our data. A shift of 4.66 GPa brings the zero pressure DFT volume into agreement with the ambient conditions data of Levien

and Prewitt (1981). Following this correction we arrive at an equation of state with parameters $V_0 = 439.1$ Å^3, $K_0 = 122.0$ GPa and $K_0' = 4.7$. This is in fair agreements with the equation of state of Levien and Prewitt (1981) ($K_0 = 113\pm3$ GPa and $K_0' = 4.7\pm7$) and gives volumes that are in good agreement with the results of Tribaudino et al. (2000) over the whole stability field of diopside (Figure 2). This agreement indicates that the calculations accurately recover the compressibility of the unit cell as a function cell volume, and this shifted equation of state should be preferred for geophysical applications based on our calculations.

The shift of the pressure scale also leads to very good agreement between the calculated internal parameters and experimental ambient pressure structure determination. In particular, if the results of the calculation at 5 GPa is compared with the structure determined by single crystal neutron-diffraction at 10 K (Prencipe et al., 2000), many calculated parameters fall within error of the equivalent experimental parameter. The largest differences are in the z parameters of the O2 and O1 positions, which differ by 7.6×10^{-4} and 3.8×10^{-4} Å (0.004 and 0.002 fractional units), respectively.

The order of the polyhedral compressibilities is the same as that found by Levien and Prewitt (1981) and Thompson and Downs (2008), with the tetrahedra being least compressible and the M2 polyhedera is most compressible, but because our data set is collected over a greater pressure range it makes sense to go beyond a measure of the linear compressibility. This

shows that the two M sites stiffen at about the same rate with increasing pressure, but the tetrahdera stiffen much more rapidly.

5 Acknowledgments

We thank NERC for funding under grants NE/C515698/1 and NE/C515704/1. AMW also gratefully acknowledges a NERC Postdoctoral Research Fellowship (NE/E012922/1), and thanks E. Palin for assistance preparing figures. The computational results in this paper were obtained using NW-GRID resources, a collaboration of Daresbury Laboratory and the Univerties of Lancaster, Liverpool and Manchester with funding from the North West Development Agency.

References

Balić Žunić, T., Makovicky, E., 1996. Determination of the centroid or 'the best center' of a coordination polyhedron. Acta Crystallographica B 52, 78–81.

Bianchi, R., Forni, A., Oberti, R., 2005. Multipole-refined charge density study of diopside at ambient conditions. Physics and Chemistry of Minerals 32, 638 – 645.

Car, R., Parrinello, M., 1985. Unified approach for molecular dynamics and density-functional theory. Physical Review Letters 86, 5727–5730.

Dove, M. T., 1989. On the computer modeling of diopside: Toward a transferable potential for silicate minerals. American Mineralogist 74, 774–779.

Gibbs, G. V., Cox, D. F., Ross, N. L., Crawford, T. D., Burt, J. B., Rosso, K. M., 2005. A mapping of the electron localization function for earth materials. Physics and Chemistry of Minerals 32, 208 – 221.

Hohenberg, P., Kohn, W., 1964. Inhomogeneous electron gas. Physical Review 136 (3B), 864 – 871.

Jung, D. Y., Oganov, A. R., 2005. Basics of first-principles simulation of matter under extreme conditions. In: Miletich, R. (Ed.), Mineral behaviour at extreme conditions. Vol. 7 of EMU Notes in Mineralogy. European Mineralogical Union, Budapest, pp. 117 – 138.

Kohn, W., Sham, L. J., 1965. Self-consistent equations including exchange and correlation effects. Physical Review 140 (4A), 1133 – 1138.

Levien, L., Prewitt, C. T., 1981. High-pressure structural study of diopside. American Mineralogist 66, 315–323.

Makovicky, E., Balić-Žunić, T., 1998. New measure of distortion for coordination polyhedra. Acta Crystallographica B 54, 766–773.

McCormick, T. C., Hazen, R. M., Angel, R. J., 1989. Compressibility of omphacite to 6- kbar: Role of vacancies. American Mineralogist 74, 1287 – 1292.

Monkhorst, H. J., Pack, J. D., Jun 1976. Special points for brillouin-zone integrations. Phys. Rev. B 13 (12), 5188–5192.

Oganov, A. R., Brodholt, J. P., Price, G. D., 2001. Ab initio elasticity and thermal equation of state of $MgSiO_3$ perovskite. Earth and Planetary Science Letters 184, 555 – 560.

Ohashi, Y., 1982 A program to calculate the strain tensor from two sets of unit-cell parameters. In: Hazen, R. M. and Finger, L. W. (Ed.), Comparative Crystal Chemistry. Wiley, New York, pp. 92-102.

Perdew, J. P., Burke, K., Emzerhof, M., 1996. Generalized gradient approximation made simple. Physical Review Letters 77, 3865 – 3868.

Prencipe, M., Tribaudino, M., Pavese, A., Hoser, A., Reehuis, M., 2000. A single-crysal neutron-diffraction investigation of diopside at 10 k. The Canadian Mineralogist 38, 183 – 189.

Segall, M. D., Lindan, P. J. D., Probert, M. J., Pickard, C. J., Hasnip, P. J., Clark, S. J., Payne, M. C., 2002. First-principles simulation: ideas, illustrations and the castep code. Journal of Physics : Condensed Matter 14, 2717 – 2743.

Thomas, J., Tyer, R. P., Allan, R. J., Dove, M. T., Austen, K. F., Walker, A. M., Bruin, R. P., Petit, L., Durrant, M. C., 2007., Science carried out as part of the NW-GRID project using the eMinerals infrastructure. Proceedings of the UK e-Science All Hands Meeting 2007, 220 – 227.

Thompson, R. M., Downs, R. T., 2001. Quantifying distortion from ideal closest-packing in a crystal structure with analysis and application. Acta Crystallographica B 57, 119–127.

Thompson, R. M., Downs, R. T., 2003. Model pyroxenes I: Ideal pyroxene topologies. American Mineralogist 88, 653–666.

Thompson, R. M., Downs, R. T., 2004. Model pyroxenes II: Structural variation as a function of tetrahederal rotation. American Mineralogist 89,

614–628.

Thompson, R. M., Downs, R. T., 2008. The crystal structure of diopside at pressure to 10 GPa. American Mineralogist 93, 177–186.

Thompson, R. M., Downs, R. T., Redhammer, G. J., 2005. Model pyroxenes III: Volume of $C2/c$ pyroxenes at mantle P, T, and x. American Mineralogist 90, 1840–1851.

Tribaudino, M., Prencipe, M., Bruno, M., Levy, D., 2000. High-presure behaviour of Ca-rich $C2/c$ clinopyroxenes along the join diopside-enstatite ($CaMgSi_2O_6$). Physics and Chemistry of Minerals 27, 656 – 664.

Vanderbilt, D., 1990. Soft self-consistent pseudopotentials in a generalized eigenvalue problem. Physical Review B 41, 7892 – 7895.

Vanderbilt, D., 1998. First-principles theory of structural phase transitions in cubic perovskites. Journal of the Korean Physical Society 32, S103 – S106.

Walker, A. M., Hermann, J., Berry, A. J., O'Neill, H. S. C., 2007. Three water sites in upper mantle olivine and the role of titanium in the water weakening mechanism. Journal of Geophysical Research 112, art. no. B05211.

Weidner, D. J., Li, L., Brodholt, J., Price, G. D., 2006. Towards a thermoelastic reference earth model. EOS transactions of the AGU, 87 (52), Fall Meeting Supplement, Abstract MR14A–01.

Zhang, L., Ahsbahs, H., Hafner, S. S., Kutoglu, A., 1997. Single-crystal compression and crystal structure of clinopyroxene up to 10 GPa. American

Mineralogist 82, 245–258.

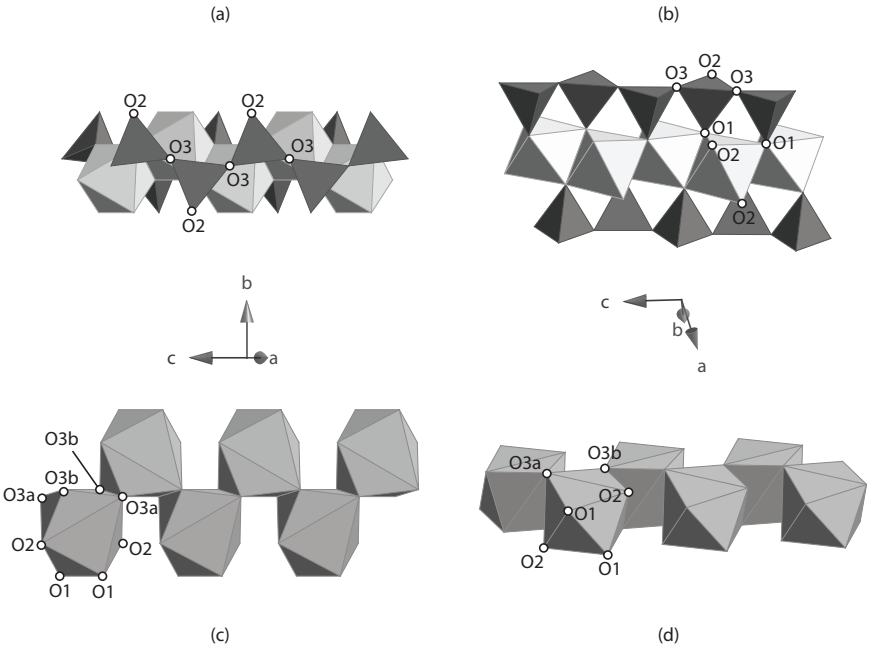

Fig. 1 Polyhedral representation of structural elements in diopside. Chains of Si tetrahedra and M1 octahedra are shown in dark grey and light grey respectively in (a) and (b) while the chains of M2 polyhedra are shown in (c) and (d).

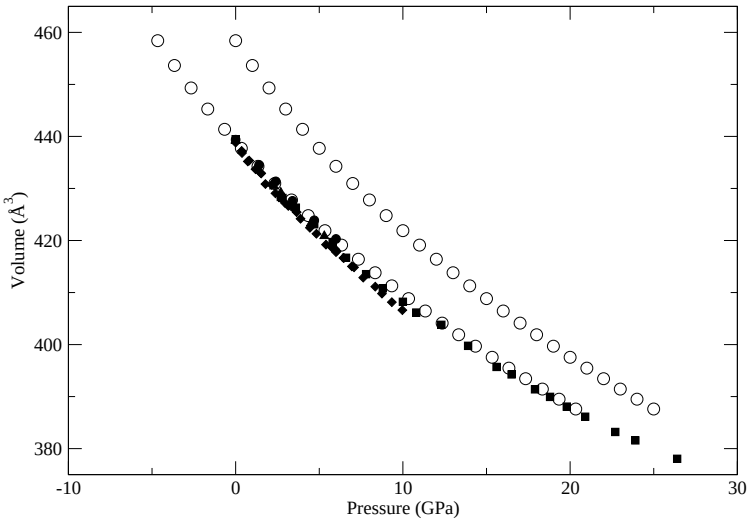

Fig. 2 Unit cell volume as a function of pressure from these calculations (open circles) and experimental studies (solid symbols; triangles: Levien and Prewitt (1981), circles: McCormick et al. (1989), diamonds: Zhang et al. (1997), squares: Tribaudino et al. (2000)). Both the original and pressure corrected DFT results are shown, with the corrected results plotting through the experimental data.

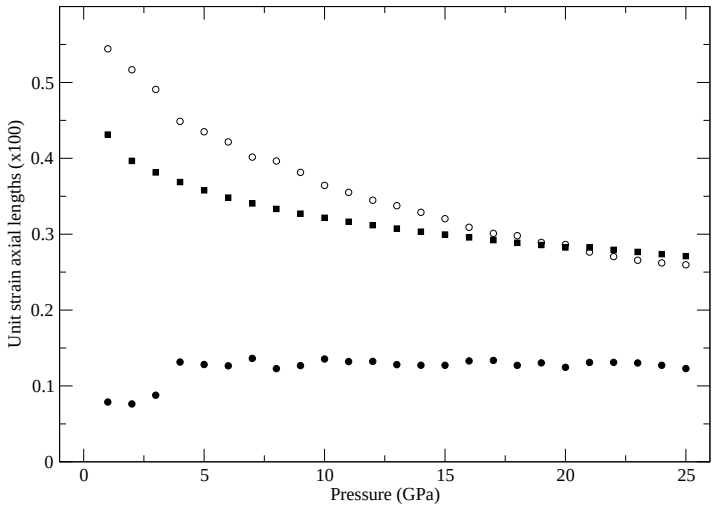

Fig. 3 Unit strain ellipsoid axial lengths as a function of pressure. Closed circles: ε_1, closed squares: ε_2, open circles: ε_3.

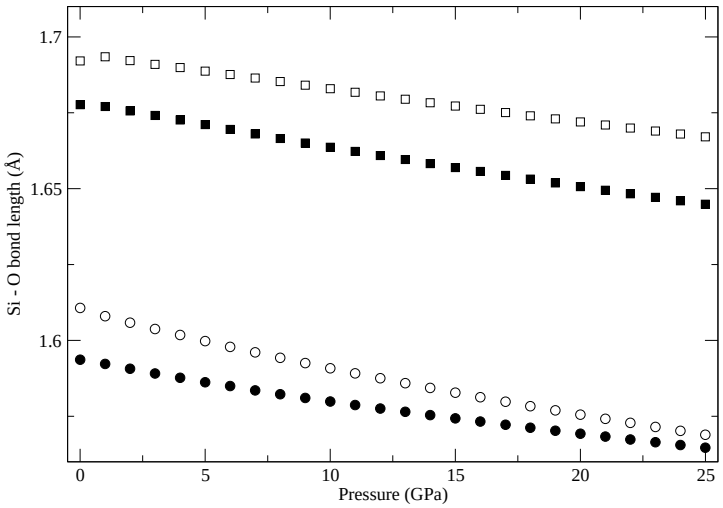

Fig. 4 Bond lengths in the Si tetrahedron as a function of pressure. Closed circles: Si–O1, open circles: Si–O2, open squares: Si–O3a, closed squares: Si–O3b.

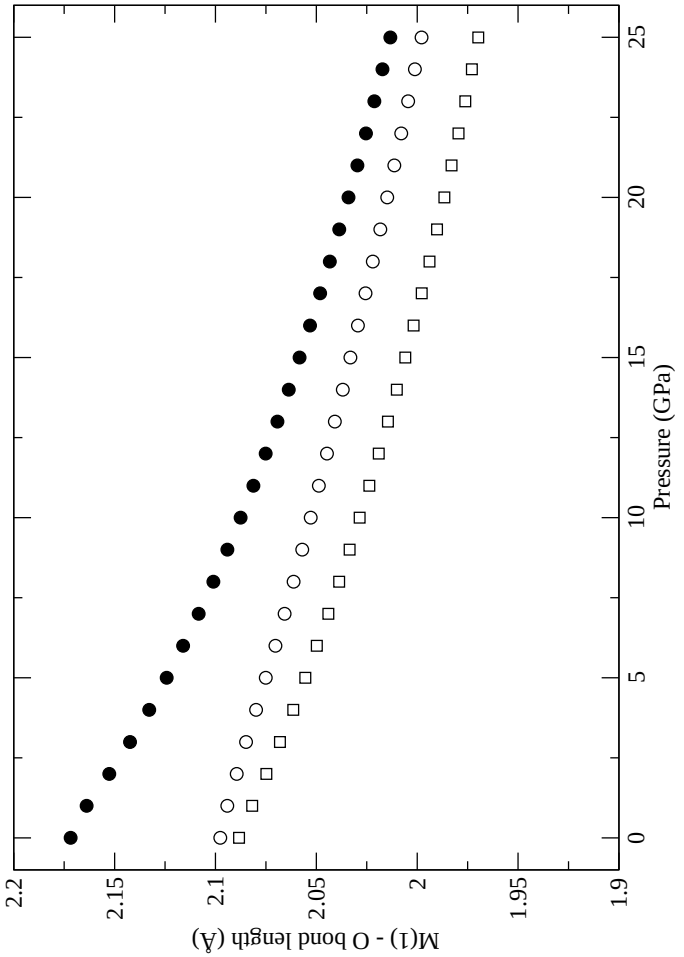

Fig. 5 Bond lengths in the M1 octahedron as a function of pressure. Open circles: Mg–O1a, closed circles: Mg-O1b, open squares: Mg–O2.

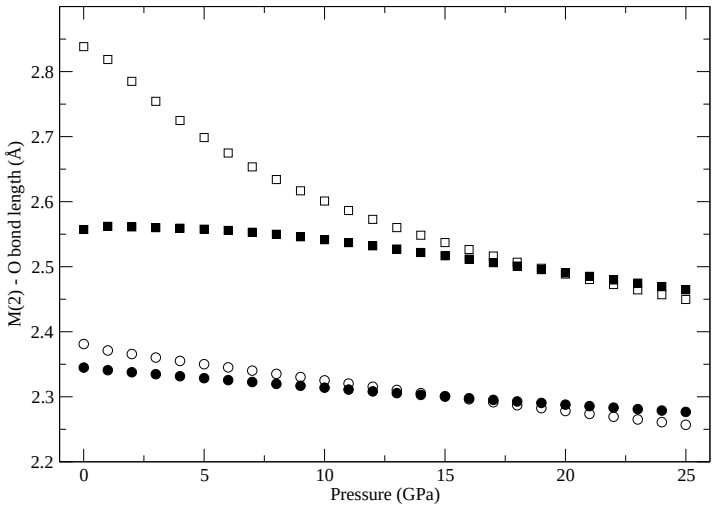

Fig. 6 Bond lengths in the M2 polyhedron as a function of pressure. Closed circles: Ca–O1, open circles: Ca–O2, open squares: Ca–O3a, closed squares: Si–O3b.

Table 1 Calculated cell parameters

P	a	b	c	β	V
0.0	9.910	9.051	5.330	106.51	458.4
1.0	9.876	9.012	5.308	106.24	453.6
2.0	9.842	8.980	5.291	106.06	449.3
3.0	9.810	8.948	5.274	105.89	445.3
4.0	9.781	8.918	5.257	105.74	441.4
5.0	9.754	8.889	5.242	105.61	437.7
6.0	9.728	8.862	5.227	105.49	434.3
7.0	9.704	8.836	5.213	105.39	431.0
8.0	9.681	8.810	5.200	105.30	427.8
9.0	9.660	8.785	5.188	105.22	424.8
10.0	9.639	8.760	5.176	105.15	421.9
11.0	9.620	8.736	5.165	105.09	419.1
12.0	9.602	8.713	5.154	105.04	416.4
13.0	9.584	8.690	5.144	104.98	413.8
14.0	9.567	8.667	5.134	104.94	411.3
15.0	9.550	8.645	5.124	104.90	408.8
16.0	9.535	8.623	5.115	104.86	406.4
17.0	9.519	8.602	5.105	104.82	404.1
18.0	9.504	8.581	5.096	104.79	401.9
19.0	9.490	8.560	5.088	104.75	399.7
20.0	9.476	8.540	5.079	104.72	397.5
21.0	9.463	8.520	5.071	104.70	395.5
22.0	9.450	8.501	5.063	104.67	393.4
23.0	9.437	8.482	5.055	104.64	391.4
24.0	9.424	8.463	5.047	104.62	389.5
25.0	9.412	8.444	5.040	104.60	387.6

Table 2 Atomic positions in the calculated structure of diopside.

P GPa	M1 y	M2 y	Si x	Si y	Si z	O1 x	O1 y	O1 z	O2 x	O2 y	O2 z	O3 x	O3 y	O3 z
0.0	0.90670	0.29872	0.28660	0.09187	0.23660	0.11713	0.08820	0.14542	0.61713	0.58820	0.14542	0.88343	0.08954	0.35370
1.0	0.90722	0.30073	0.28616	0.09308	0.23544	0.11662	0.08926	0.14563	0.61662	0.58926	0.14563	0.88338	0.08926	0.35437
2.0	0.90765	0.30135	0.28627	0.09337	0.23456	0.11653	0.08934	0.14546	0.61652	0.58934	0.14546	0.88347	0.08934	0.35455
3.0	0.90803	0.30192	0.28635	0.09365	0.23371	0.11643	0.08942	0.14527	0.61643	0.58942	0.14527	0.88357	0.08942	0.35474
4.0	0.90836	0.30250	0.28640	0.09393	0.23279	0.11631	0.08952	0.14504	0.61631	0.58952	0.14504	0.88369	0.08952	0.35496
5.0	0.90867	0.30301	0.28644	0.09418	0.23198	0.11621	0.08962	0.14483	0.61621	0.58962	0.14483	0.88379	0.08962	0.35517
6.0	0.90894	0.30348	0.28648	0.09443	0.23124	0.11610	0.08971	0.14464	0.61610	0.58971	0.14464	0.88390	0.08971	0.35536
7.0	0.90919	0.30389	0.28652	0.09463	0.23063	0.11600	0.08980	0.14446	0.61600	0.58980	0.14446	0.88400	0.08980	0.35554
8.0	0.90942	0.30426	0.28656	0.09483	0.23012	0.11589	0.08989	0.14430	0.61589	0.58989	0.14430	0.88411	0.08989	0.35570
9.0	0.90964	0.30461	0.28658	0.09503	0.22976	0.11579	0.08998	0.14416	0.61579	0.58998	0.14416	0.88421	0.08998	0.35585
10.0	0.90984	0.30494	0.28658	0.09523	0.22951	0.11568	0.09009	0.14402	0.61568	0.59009	0.14402	0.88432	0.09009	0.35597
11.0	0.91002	0.30525	0.28659	0.09541	0.22931	0.11558	0.09019	0.14390	0.61558	0.59019	0.14390	0.88442	0.09019	0.35609
12.0	0.91020	0.30555	0.28659	0.09559	0.22917	0.11547	0.09030	0.14378	0.61547	0.59030	0.14378	0.88453	0.09030	0.35622
13.0	0.91037	0.30584	0.28658	0.09578	0.22907	0.11536	0.09041	0.14366	0.61536	0.59042	0.14367	0.88464	0.09041	0.35634
14.0	0.91053	0.30612	0.28657	0.09595	0.22901	0.11525	0.09053	0.14355	0.61525	0.59053	0.14355	0.88475	0.09054	0.35645
15.0	0.91069	0.30638	0.28656	0.09614	0.22897	0.11515	0.09066	0.14342	0.61515	0.59066	0.14342	0.88485	0.09065	0.35657
16.0	0.91084	0.30664	0.28654	0.09632	0.22894	0.11505	0.09078	0.14331	0.61505	0.59078	0.14331	0.88495	0.09078	0.35669
17.0	0.91099	0.30689	0.28652	0.09649	0.22895	0.11494	0.09090	0.14318	0.61494	0.59091	0.14318	0.88506	0.09090	0.35681
18.0	0.91113	0.30712	0.28650	0.09667	0.22896	0.11484	0.09102	0.14306	0.61484	0.59103	0.14306	0.88516	0.09102	0.35693
19.0	0.91127	0.30739	0.28646	0.09684	0.22897	0.11473	0.09118	0.14292	0.61473	0.59118	0.14292	0.88527	0.09118	0.35708
20.0	0.91140	0.30758	0.28645	0.09700	0.22906	0.11465	0.09128	0.14281	0.61465	0.59128	0.14281	0.88535	0.09128	0.35719
21.0	0.91152	0.30780	0.28643	0.09717	0.22913	0.11455	0.09141	0.14268	0.61455	0.59141	0.14268	0.88545	0.09140	0.35732
22.0	0.91164	0.30803	0.28639	0.09733	0.22928	0.11445	0.09154	0.14256	0.61445	0.59154	0.14256	0.88555	0.09154	0.35744
23.0	0.91176	0.30823	0.28637	0.09749	0.22932	0.11436	0.09166	0.14241	0.61436	0.59166	0.14241	0.88564	0.09166	0.35758
24.0	0.91187	0.30844	0.28634	0.09764	0.22944	0.11427	0.09179	0.14228	0.61426	0.59179	0.14228	0.88573	0.09179	0.35772
25.0	0.91197	0.30864	0.28630	0.09781	0.22956	0.11417	0.09193	0.14214	0.61417	0.59193	0.14214	0.88583	0.09192	0.35785

Table 3 The effect of pressure on some measures of structural regularity

P GPa	O3O3O3	Δ_{Si} Å	υ_{Si} (%)	Δ_{Mg} Å	Σ_{Mg}	υ_{Mg} (%)	Δ_{Ca} Å	Σ_{Ca}	υ_{Ca} (%)
0.0	170.02	0.0779	0.4631	0.0605	0.9929	0.5845	0.2628	0.9439	1.3607
1.0	168.57	0.0776	0.4356	0.0572	0.9939	0.5801	0.2403	0.9506	1.3604
2.0	167.62	0.0778	0.4195	0.0543	0.9949	0.5723	0.2306	0.9551	1.3802
3.0	166.76	0.0781	0.4067	0.0519	0.9958	0.5668	0.2223	0.9592	1.4014
4.0	165.93	0.0781	0.3968	0.0499	0.9965	0.5648	0.2146	0.9631	1.4249
5.0	165.21	0.0784	0.3881	0.0480	0.9970	0.5641	0.2079	0.9665	1.4502
6.0	164.58	0.0785	0.3812	0.0464	0.9975	0.5652	0.2020	0.9694	1.4749
7.0	164.04	0.0786	0.3763	0.0450	0.9980	0.5670	0.1967	0.9720	1.4969
8.0	163.55	0.0787	0.3721	0.0436	0.9985	0.5702	0.1920	0.9742	1.5169
9.0	163.14	0.0787	0.3691	0.0424	0.9989	0.5751	0.1879	0.9760	1.5311
10.0	162.78	0.0787	0.3673	0.0413	0.9992	0.5816	0.1841	0.9776	1.5396
11.0	162.45	0.0787	0.3664	0.0403	0.9996	0.5893	0.1806	0.9790	1.5470
12.0	162.16	0.0787	0.3667	0.0393	0.9999	0.5985	0.1774	0.9803	1.5510
13.0	161.89	0.0787	0.3673	0.0384	0.9998	0.6092	0.1744	0.9815	1.5531
14.0	161.66	0.0787	0.3685	0.0375	0.9995	0.6221	0.1715	0.9825	1.5522
15.0	161.43	0.0786	0.3708	0.0368	0.9993	0.6350	0.1688	0.9835	1.5505
16.0	161.23	0.0786	0.3736	0.0360	0.9991	0.6498	0.1663	0.9844	1.5472
17.0	161.04	0.0786	0.3769	0.0353	0.9989	0.6662	0.1638	0.9852	1.5420
18.0	160.88	0.0786	0.3801	0.0346	0.9987	0.6836	0.1615	0.9860	1.5382
19.0	160.72	0.0786	0.3856	0.0340	0.9986	0.7037	0.1592	0.9868	1.5280
20.0	160.55	0.0785	0.3892	0.0334	0.9984	0.7220	0.1571	0.9875	1.5223
21.0	160.40	0.0785	0.3942	0.0328	0.9983	0.7430	0.1551	0.9881	1.5139
22.0	160.29	0.0785	0.4004	0.0322	0.9982	0.7667	0.1531	0.9888	1.5009
23.0	160.13	0.0784	0.4054	0.0317	0.9981	0.7887	0.1512	0.9894	1.4941
24.0	160.01	0.0784	0.4119	0.0312	0.9980	0.8135	0.1493	0.9900	1.4819
25.0	159.89	0.0783	0.4183	0.0307	0.9980	0.8392	0.1475	0.9906	1.4702